Extended model of the channel diffusivity in the rutile structure

K. Ruebenbauer,* U. D. Wdowik, M. Kwater, and J. T. Kowalik
Institute of Physics and Computer Science, Pedagogical University, PL-30-084 Cracow, ul. Podchorążych 2, Poland
(Received 4 June 1993; revised manuscript received 5 August 1996)

A model describing the diffusivity of a highly diluted and randomly distributed substitutional cationic impurity via the open and almost empty ⟨001⟩ channels in the rutile structure has been developed recently. The above model is based upon the assumption that the insignificant fraction of the impurities resides in the channels. An extended model is developed that allows for a significant fraction of the impurities to stay within channels, and it is used to evaluate emission Mössbauer spectra originating from the diffusing impurities embedded in single-crystalline samples. Final results are shown for the 14.4-keV Mössbauer line in ^{57}Co(Fe). It is shown that spectral line positions depend upon the wave-vector transfer to the system, and that the data are sensitive to the fraction of both parent and daughter impurities residing in the channels. [S0163-1829(96)05442-2]

I. INTRODUCTION

Measurements of the diffusion coefficient tensor for highly diluted and randomly distributed substitutional cationic impurities in the rutile structure (an almost stoichiometric TiO_2 rutile is a well-known example) indicate for many such impurities a very large anisotropy, with the diffusivity being much larger along the tetragonal axis as compared to the diffusivity in the tetragonal plane.[1] The anisotropy could be explained by invoking a rapid diffusive motion of the impurities along the open and almost empty ⟨001⟩ channels.[1] A model of such a mechanism has recently been developed from the ''first principles,'' and discussed extensively in the literature.[2] The basic feature of the above model is the assumption that the insignificant fraction of the impurities resides in the channel sites called further (C) sites and, hence, no measurable signal comes from the (C) sites.[2] Such an assumption seems natural in the case of the host cations, as otherwise no empty channels exist, and the lattice becomes susceptible to the collapse. However, very highly diluted cationic impurities do not need to follow the above pattern as far as the lattice stability and the channel emptiness are concerned. Hence, the above-mentioned assumption could be relaxed for diluted impurities leading to the extended model of the channel diffusivity, the latter exhibiting a rich manifold of the possible eigensolutions.

The last model allows us to account for the possible aftereffects in a straightforward manner. That is, a distribution of impurities between (C) sites and regular cationic sites called further (R) sites does not need to be the same for parent and daughter radioactive impurities, e.g., Mössbauer parent and daughter atoms in the case of emission Mössbauer spectroscopy, provided these impurities are different elements, e.g., Co parent and Fe daughter. The model is sensitive to both of the above distributions provided a time scale for the evolution from one to another is comparable with the time window of the experimental method, i.e., with the Mössbauer level lifetime in the case of the emission Mössbauer spectroscopy. Due to the fact that some diffusive jumps occur between two different Bravais sublattices (R) and (C) leading to a simultaneous relaxation of the hyperfine interactions, spectral line positions of the Mössbauer emission profile depend upon the wave-vector transfer to the system, i.e., upon the orientation of the single crystal sample versus the emitted γ-ray. Such behavior has not been predicted previously, to our best knowledge.

The paper is organized as follows: Sec. II deals with the extension of the previous two-state model (2SM) (Ref. 2) to the extended three-state model (3SM). Section III discusses thermodynamics of the 3SM, while Sec. IV is devoted to some examples of the possible Mössbauer spectra calculated for the 14.4-keV Mössbauer line in ^{57}Co(Fe) in the case of emission spectroscopy from single crystals. The summary of results is given in Sec. V.

II. EXTENDED MODEL OF THE DIFFUSIVITY/RELAXATION

In order to evaluate observable quantities, one has to start with the evaluation of the appropriate diffusion/relaxation matrix leading to the superoperator describing the problem. Figure 1 shows details of the rutile structure and diffusive jumps of the cationic impurity. One can assume that anions fill almost completely their sublattice, and remain practically immobile as far as the diffusivity is concerned. Host cations almost fill a tetragonal body-centered Bravais sublattice having a chemical unit cell with the lattice constant a in the tetragonal plane, and the lattice constant c along the tetragonal axis. A very small fraction of the host cations remains in the (C) sites, moving rapidly along the ⟨001⟩ channels and exchanging with the host atoms in the (R) sites via the predominantly interstitialcy mechanism. Hence a small fraction of randomly distributed vacancies is left in the (R) sites to account for the overall charge neutrality.

Diluted cationic impurities (both parent and daughter) are distributed randomly between (R) and (C) sites, changing slightly the concentration of the (R) vacancies and interstitial host cations in the case when their charges are different from charges of the host cations. (C) sites form an almost empty (impurities are very diluted) simple tetragonal Bravais sublattice having a chemical unit cell of the dimensions $a/\sqrt{2}$ and $c/2$, respectively. The latter sublattice is rotated by $\pi/4$

 © 1996 The American Physical Society

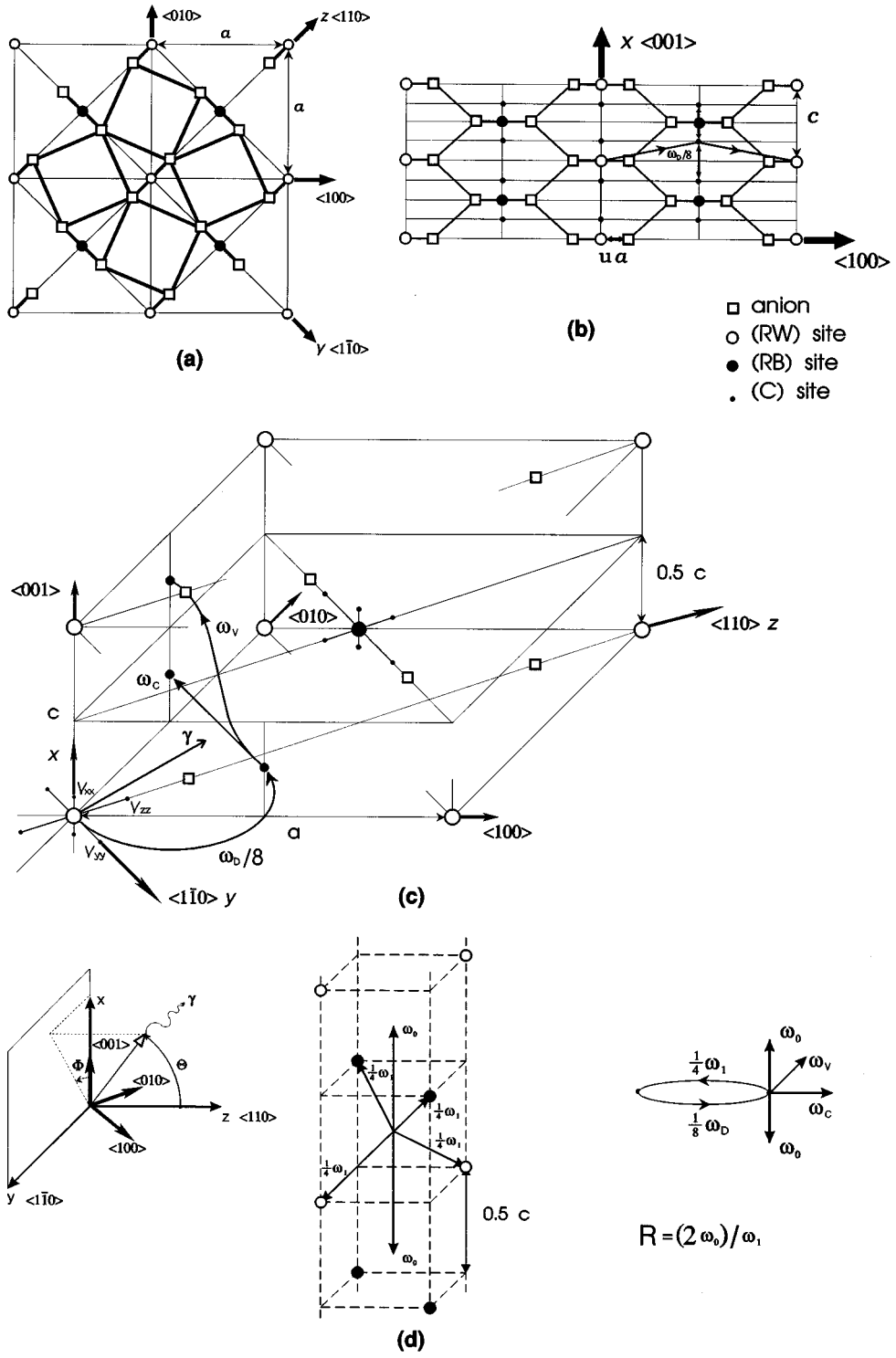

FIG. 1. Details of the rutile structure: (a) View ''down'' the tetragonal axis. (b) ''Side'' view. (c) ''Panoramic'' view of the chemical unit cell. (d) Adopted polar θ and azimuthal ϕ angles shown in respect to the crystal axes; ''panoramic'' view of the $\langle 001 \rangle$ channel and diagram of the impurity jumps: u stands for the oxygen parameter (Ref. 2), while the remaining symbols are explained within the text. Usually $u \cong 0.3$.

around the tetragonal axis and shifted by $[\frac{1}{2}\ 0\ \frac{1}{4}]$ in the crystallographic coordinates of the sublattice (R). Hence there are two (C) sites per each (R) site. A sublattice (R) splits into two simple tetragonal Bravais sublattices: white (RW) and black (RB) as far as the orientation of the local tensors is concerned. (RW) and (RB) sites transform one into another by a right-angle rotation around the tetragonal axis. Due to the fact that (R) sites have inversion centers, the lowest rank (order) of the relevant tensors equals two (it is assumed that magnetic interactions are absent). One has to note that the (C) sublattice splits into four sublattices as far as the accessibility of the adjacent (R) and (C) sites is considered. That is one can distinguish bottom sites (b) located in the crystallographic plane $[0\ 0\ \frac{1}{4}]$ and top sites (t) located

in the plane $[0\ 0\ \frac{3}{4}]$ as far as the jump routes to the adjacent (C) sites are concerned. A further splitting within each of the above (and all equivalent) planes is caused by the accessibility of the (R) sites; i.e., sites $[\frac{1}{2}\ 0\ \frac{1}{4}]$ and $[\frac{1}{2}\ 1\ \frac{1}{4}]$ differ from sites $[0\ \frac{1}{2}\ \frac{1}{4}]$ and $[1\ \frac{1}{2}\ \frac{1}{4}]$, while sites $[\frac{1}{2}\ 0\ \frac{3}{4}]$ and $[\frac{1}{2}\ 1\ \frac{3}{4}]$ differ from sites $[0\ \frac{1}{2}\ \frac{3}{4}]$ and $[1\ \frac{1}{2}\ \frac{3}{4}]$. There is no inversion center on the (C) sites. However, a symmetry breaking between various (C) sites is of the very mild character as it solely affects odd tensors having rank (order) higher than two.[3] Hence one can treat all (C) sites as equivalent, provided a recoilless fraction is taken in the quadratic approximation and magnetic interactions are absent.

A common orthogonal coordinate frame $[xyz]$, with the x axis parallel to $\langle 001\rangle$, the y axis parallel to $\langle 110\rangle$, and the z axis parallel to $\langle 110\rangle$ assures that all second-rank (order) tensors involved are diagonal [see Fig. 1(c) for the orientation of the electric-field gradient tensor (EFG) principal components V_{xx}, V_{yy}, and V_{zz} on the (RW) site]. Figure 1(d) shows related polar θ and azimuthal ϕ angles defining the direction of the emitted γ ray. Due to the fact that (R) sites have inversion centers and all (C) sites forming a tetragonal sublattice are equivalent in the present context, one can take a wave-vector transfer to the lattice as the wave vector of the emitted photon.

Daughter impurity jumps are described by the following frequencies: ω_D stands for the jump frequency from the (R) site into any adjacent (C) site. It is assumed that these jumps occur mainly via the interstitialcy mechanism; i.e., a cation (mainly a host cation) traveling along the channel moves into the vicinity of the impurity and kicks it into any of the adjacent channel sites, filling its place. Due to the fact that each (R) site is surrounded by eight (C) sites, a particular jump occurs with the frequency $\frac{1}{8}\omega_D$. There are no direct (R) to (R) jumps. It has to be realized that the above jumps are correlated events involving ''simultaneous'' jumps of two atoms [a host atom jumps into an (R) site, and an impurity jumps ''simultaneously'' into a (C) site]. A daughter impurity within a channel could jump to the adjacent (empty) cell with the frequency ω_0. There are two such jumps possible, as two channel cells are adjacent to each (C) site. Additionally, an impurity can jump to the adjacent (empty) channel within a tetragonal plane with the frequency ω_c [there are four such routes possible for each (C) site] and out of the tetragonal plane with the frequency ω_v [see Fig. 1(c) for details]. There are four routes for ω_v jumps, as the remaining four are blocked by the host cation-anion bond. Finally, an impurity can jump into any adjacent (R) site via the interstitialcy mechanism, kicking the (R) cation (mainly a host cation) into any surrounding channel. The evicted cation moves away along the channel quite rapidly. The last event is again a correlated event involving two atoms, and it occurs with the frequency ω_1. Hence a particular jump occurs with the frequency $\frac{1}{4}\omega_1$ as each (C) site is surrounded by four (R) sites. All jumps within the (C) sublattice are single-atom jumps, as the latter sublattice remains practically empty. Figure 1(d) shows a schematic diagram of jumps originating from the (C) site. It is convenient to define the following ratio: $R=(2\omega_0)/\omega_1$.[2]

One has to note that (RW) and (RB) sites differ solely by the orientation of the second rank (order) and higher tensors, while the (C) site is characterized by its own recoilless fraction, total shift and EFG (higher tensors are neglected). All second-rank (order) tensors on the (C) sites are axially symmetric, with the symmetry axis being parallel to the tetragonal axis. 50% of the ω_1 jumps from the (C) sites lead an impurity to the (RW) sites, and 50% to the (RB) sites.

Hence a diffusion/relaxation matrix has dimensions $[3\otimes 3]$ as the impurity can reside either in (RW) or (RB) or (C) sites. A relaxation matrix $\hat{W}_R$ takes on the following form:[2,4–6]

$$\hat{W}_R=\begin{pmatrix} -\omega_D & 0 & \omega_D \\ 0 & -\omega_D & \omega_D \\ \frac{1}{2}\omega_1 & \frac{1}{2}\omega_1 & -\omega_1 \end{pmatrix}, \tag{1}$$

where the first row represents an (RW) sublattice, the second row an (RB) sublattice and the third row (C) sublattice. One has to note, that the $\hat{W}_R$ matrix is a nonsymmetric matrix, in general. A corresponding diffusivity matrix $\hat{W}_D$ takes on the form[2,6–9]

$$\hat{W}_D=\begin{pmatrix} -\omega_D & 0 & \omega_D\alpha_1 \\ 0 & -\omega_D & \omega_D\alpha_1 \\ \frac{1}{2}\omega_1\alpha_1^* & \frac{1}{2}\omega_1\alpha_1^* & W_{33}^{(D)} \end{pmatrix}. \tag{2}$$

A geometrical factor α_1 represents all jumps leading from (R) to (C) sublattice. One has to note that the same factor describes jumps originating at the (RW) and (RB) sites, as both of them belong to the same Bravais sublattice and differ one from another solely by color.[2] Due to the fact that (R) sites possess inversion centers, the factor α_1 is a real number. Off-diagonal elements of the third row of the matrix $\hat{W}_D$ represent all the jumps originating on any (C) site, and leading either to the (RW) site (first element) or to the (RB) site (second element). Due to the fact that (C) sites constitute a Bravais sublattice, while (R) sites constitute another Bravais sublattice, both geometrical factors of the above-mentioned off-diagonal elements equal α_1^* (in fact they equal α_1 for the case considered, as α_1 is a real number). A geometrical factor α_1 takes on the following form:

$$\alpha_1=\tfrac{1}{8}\sum_{i=1}^{8}\cos(\overline{q}\cdot\overline{R_i}), \tag{3}$$

where $\overline{q}$ stands for the wave-vector transfer to the system, and R_i denotes a jump vector. Jump vectors of the α_1 factor could be expressed as follows in the coordinates $[xyz]$

$$\begin{gathered} \overline{R_1}=(XYZ),\quad \overline{R_2}=(-XYZ),\quad \overline{R_3}=(X-YZ), \\ \overline{R_4}=(-X-YZ), \\ \overline{R_5}=(XY-Z),\quad \overline{R_6}=(-XY-Z),\quad \overline{R_7}=(X-Y-Z), \\ \overline{R_8}=(-X-Y-Z) \end{gathered} \tag{4}$$

with $X=\frac{1}{4}c$ and $Y=Z=a/(2\sqrt{2})$.

A matrix element $W_{33}^{(D)}$ describes all jumps within a (C) Bravais sublattice and a decay of the (C) state due to the jumps leading to the (R) state. Hence it takes on the following form:

$$W_{33}^{(D)} = -\omega_1[1+R(1-\alpha_3)] - 4\omega_c[1-\alpha_3^{(c)} - 4\omega_v(1-\tfrac{1}{2}(\alpha_3^{(b)}+\alpha_3^{(t)})]. \quad (5)$$

A geometrical factor α_3 represents jumps within a channel, the latter forming a subgroup having an inversion center.[2] Hence this factor can be expressed in the following way:[2]

$$\alpha_3 = \sum_n \rho_n \cos(\overline{q}\cdot\overline{R}_n),$$

where $\overline{R}_n = ((n/2)c\ 0\ 0)$ in the $[xyz]$ frame, and

$$\rho_n = \exp[-\tfrac{1}{2}(n/\sigma)]/\sum_{n'} \exp[-\tfrac{1}{2}(n'/\sigma)], \quad (6)$$

with $n=0,1,2,\ldots$. The parameter σ depends solely upon the frequency ratio R, and it is described by expression (13) of Ref. 2.

A factor $\alpha_3^{(c)}$ describes jumps from the (C) site into any adjacent (C) site within the same tetragonal plane. These jumps also form a subgroup which is symmetrical against inversion. Hence, the factor $\alpha_3^{(c)}$ takes on the form

$$\alpha_3^{(c)} = \tfrac{1}{4}\sum_{i=1}^{4} \cos(\overline{q}\cdot\overline{R}_i^{(c)}),$$

with the following jump vectors in the $[xyz]$ frame:

$$\overline{R}_1^{(c)} = (0\,Y_c\,0), \quad \overline{R}_2^{(c)} = (0\,-Y_c\,0), \quad \overline{R}_3^{(c)} = (0\,0\,Z_c), \quad \overline{R}_4^{(c)} = (0\,0\,-Z_c), \quad (7)$$

where $Y_c = Z_c = a/\sqrt{2}$. The last two factors $\alpha_3^{(b)}$ and $\alpha_3^{(t)}$ represent ω_v jumps originating at the (b) and (t) sites, respectively. Neither the (b) nor (t) subgroup has an inversion center, however the average of both of them is invariant against inversion [there is the same probability of finding an impurity at either the (b) or (t) site]. Hence the factor $\alpha_3^{(t)}$ can be obtained as $\alpha_3^{(t)} = [\alpha_3^{(b)}]^{\star}$, while the factor $\alpha_3^{(b)}$ follows the expression

$$\alpha_3^{(b)} = \tfrac{1}{4}\sum_{i=1}^{4} \exp[i\overline{q}\cdot\overline{R}_i^{(b)}],$$

with the following jump vectors in the $[xyz]$ frame:

$$\overline{R}_1^{(b)} = (X_c\,Y_c\,0), \quad \overline{R}_2^{(b)} = (X_c\,-Y_c\,0), \quad \overline{R}_3^{(b)} = (-X_c\,0\,Z_c), \quad \overline{R}_4^{(b)} = (-X_c\,0\,-Z_c), \quad (8)$$

where $X_c = c/2$.

A total diffusivity/relaxation operator equals $\hat{W} = \tfrac{1}{2}(\hat{W}_R + \hat{W}_D)$. One has to note that the presence of the ω_c and/or ω_v jumps leads to ''delocalized channels.'' The operators $\hat{W}_R$ and $\hat{W}_D$ are defined in the same ''Hilbert space,'' as all the relaxation processes are driven here by the diffusive motions.

In order to proceed further one needs to define occupancies of the respective sites, i.e., (RW), (RB), and (C) sites by the daughter impurity. It is obvious that occupancies of the (RW) and (RB) sites are equal each to other as those sites belong to the same Bravais sublattice. The sum of the occupancies is constant at any instant of non-negative time as the daughter particles are conserved once they are born in the radioactive decay occurring at the ''zero'' time (it is practical to normalize occupancies to unity). Hence occupancies of the respective sites could be expressed as follows:

$$p_1 = p_2 \quad \text{and} \quad p_1 + p_2 + p_3 = 1, \quad \text{with } p_1 > 0, \quad p_2 > 0 \quad \text{and} \quad p_3 > 0, \quad (9)$$

where p_1, p_2, and p_3 stand for the occupancies of the (RW), (RB), and (C) sites, respectively. Due to the above conditions only a single parameter remains free, e.g., $0 < p_3 < 1$. One has to note, that the probability p_3 does not need to be the same for the parent and daughter atoms. For impurities remaining at equilibrium between (R) and (C) sublattices a probability p_3 obeys the relationship

$$p_\infty^{(3)} = \omega_D/(\omega_D + \omega_1), \quad (10)$$

where the symbol $p_\infty^{(3)}$ denotes a probability p_3 at equilibrium. Hence for a limiting case $\omega_1 \gg \omega_D$ one obtains the 2SM model with $p_\infty^{(3)} \Rightarrow 0$.

A diffusion coefficient tensor of the 3SM model is diagonal in the crystallographic and $[xyz]$ coordinates, and it has an axial symmetry around the tetragonal axis. Its components obey the following relationships:

$$D\langle 100\rangle = \tfrac{1}{2}[\tfrac{1}{4}\omega_S + p_\infty^{(3)}(\omega_c+\omega_v)]a^2, \quad D\langle 010\rangle = D\langle 100\rangle, \quad D\langle 001\rangle = \tfrac{1}{2}\left(\tfrac{1}{8}\,\omega_S\left[\sum_{n=0}^{\infty}\{\rho_n[2n(n+1)+1]\}\right] + p_\infty^{(3)}\omega_v\right)c^2, \quad (11)$$

with $\omega_S = (\omega_D\omega_1)/(\omega_D+\omega_1)$, where $D\langle 100\rangle$, $D\langle 010\rangle$, and $D\langle 001\rangle$ stand for diffusion coefficients along the $\langle 100\rangle$, $\langle 010\rangle$ and $\langle 001\rangle$ axes, respectively. An average diffusion coefficient equals $\langle D\rangle = \tfrac{1}{3}\{D\langle 001\rangle + 2D\langle 100\rangle\}$, while a diffusion coefficient in the arbitrary direction $\theta\phi$ is expressed as follows:[2]

$$D(\theta\phi) = D\langle 001\rangle \sin^2\theta\,\cos^2\phi + D\langle 100\rangle \times (\sin^2\theta\,\sin^2\phi + \cos^2\theta). \quad (12)$$

The above diffusion coefficient tensor reduces to the tensor of the 2SM model for $\omega_1 \gg \omega_D$ and $\omega_c = \omega_v = 0$. Due to the fact that the diffusion coefficient is obtained by averaging over many jumps, it is justified to use equilibrium occupancies and a weighted average (effective) frequency ω_S, the latter being a scaling frequency for jumps between various Bravais sublattices. One has to note that ω_S approaches ω_D in the 2SM model, as for the latter case a condition $\omega_1 \gg \omega_D$ is satisfied.

For relatively short observation times, i.e., for an emission Mössbauer spectroscopy, where the observation time is defined by the Mössbauer level lifetime, one can expect even at the local scale an evolution of the p_3 parameter from the equilibrium value for the parent atom to the equilibrium value $p_\infty^{(3)}$ of the daughter atom, as the parent atom lives long enough to reach a local equilibrium prior to decay. For such an after effect to occur equilibrium conditions have to be different for parent and daughter atoms, i.e., those atoms have to be different elements. A Mössbauer emission experi-

ment is being performed in reciprocal space-time and, hence, one has to use the following weighted average for the p_3 occupancy:

$$p_3=[\Gamma_0/(\Gamma_0+\omega_D+\omega_1)](p_0^{(3)}-p_\infty^{(3)})+p_\infty^{(3)}, \quad (13)$$

where Γ_0 stands for the natural linewidth of the Mössbauer excited level in the (C) site, and $p_0^{(3)}$ denotes the probability to find a daughter Mössbauer atom in the (C) site at the instant of the formation of the Mössbauer level. Remaining occupancies p_1 and p_2 follow from Eq. (9). One can see immediately that in the ''static'' limit an experiment is sensitive to the parent atoms distribution, while in the fast diffusion limit the same experiment is sensitive to the daughter atom distribution. It is assumed that other after effects decay at a very short-time interval.

Due to the fact that magnetic hyperfine interactions are absent and the crystal-field level splitting is much larger than the hyperfine interactions, it is justified to take super-Hamiltonians in the semiclassical approximation. It is justified as well to assume that all hyperfine levels are thermally equalized at relevant temperatures. Super-Hamiltonians of sites (RW) and (RB) are the same as in the 2SM model (see Ref. 2), while the matrix element of the super-Hamiltonian of the (C) site takes on the form

$$H_3^x(m_e m_g m_e' m_g')=\delta(m_e m_e')H_g^{(3)}(m_g m_g')-\delta(m_g m_g')\times[H_e^{(3)}(m_e m_e')+\delta(m_e m_e')S^{(3)}], \quad (14)$$

where the indices e and g refer to the excited and ground nuclear states, respectively; m_e and m_g stand for the respective magnetic quantum numbers; $H_g^{(3)}(m_g m_g')$ and $H_e^{(3)}(m_e m_e')$ stand for the matrix elements of the nonscalar ground and excited hyperfine Hamiltonians; and $S^{(3)}$ denotes a total shift at the site (C), which is generally different from the shift at the site (R) as these sites belong to different Bravais sublattices. A Hamiltonian $\hat{H}^{(3)}$ takes on the following form in the frame $[xyz]$ upon having dropped indices e and g for brevity:

$$\hat{H}^{(3)}=A_{xx}^{(3)}[3\hat{I}_x^2-\hat{I}^2], \quad (15)$$

where $\hat{I}_x$ stands for the nuclear-spin projection operator on the x axis, $\hat{I}$ stands for the total nuclear spin operator, and $A_{xx}^{(3)}$ denotes a quadrupole coupling constant

$$A_{xx}^{(3)}=\left(\frac{\mathbf{e}Q}{4I(2I-1)}\right)V_{xx}^{(3)},$$

where $\mathbf{e}$ denotes an elementary positive charge, I stands for the nuclear spin, Q stands for the nuclear quadrupole moment and $V_{xx}^{(3)}$ denotes an electric field gradient along the tetragonal axis at the (C) site. A simple form of the Hamiltonian $\hat{H}^{(3)}$ is due to the fact that (C) sites exhibit an axial symmetry around the tetragonal axis as long as the second-order (rank) tensors are concerned.

A recoilless fraction at the (C) site again has an axial symmetry around the tetragonal axis as far as the quadratic approximation holds.[2] Recoilless fractions for the (RW) and (RB) sites are the same as in the 2SM model (see Ref. 2). Hence a recoilless fraction at the (C) site obeys the following expression in the $[xyz]$ frame:

$$f_3(\overline{q})=\exp(-q_0^2[B_{xx}^{(3)}(\sin\theta\cos\phi)^2+B_{zz}^{(3)}\times[(\cos\theta)^2+(\sin\theta\cos\phi)^2]]), \quad (16)$$

where q_0 stands for the absolute value of the wave-vector transfer, $B_{xx}^{(3)}$ stands for the mean squared displacement along the tetragonal axis, and $B_{zz}^{(3)}$ stands for the mean-squared displacement perpendicular to the tetragonal axis.

The average effective recoilless fraction (averaged over sites) follows the expression[2]

$$f_S(\overline{q})=\lambda^{-1}[p_1 f_1(\overline{q})+p_2 f_2(\overline{q})+p_3 f_3(\overline{q})], \quad (17)$$

where λ stands for the background correction factor defined in Ref. 2.

A vibrational dynamical matrix elements[2] take on the following form in the independent dynamics approximation:

$$f_{ss'}(\overline{q})=(f_s(\overline{q})f_{s'}(\overline{q}))^{1/2}, \quad (18)$$

where the indices s and s' enumerate respective sites, i.e., (RW), (RB), and (C) sites. One has to note, that the above matrix is real and symmetrical.

The above-mentioned information constitutes a complete 3SM model. One can conclude that the extension from the 2SM model to the 3SM model could be achieved by introducing the following parameters absent in the 2SM model: $V_{xx}^{(3)}$, an electric-field gradient at (C) site along the x axis; $S^{(3)}$, a total spectral shift at the (C) site; $B_{xx}^{(3)}$, a mean-squared displacement along the x axis at (C); $B_{zz}^{(3)}$, a mean-squared displacement perpendicular to x axis at (C); ω_1, a jump frequency from a (C) site to any (R) site; $p_0^{(3)}$, an occupancy of the (C) site by a daughter atom at instant of its birth; ω_c, a direct jump frequency from a (C) site to another (C) site in the tetragonal plane; and ω_v, a direct jump frequency from a (C) site to another (C) site in the adjacent channel with the ''vertical'' component. All previous parameters of the 2SM model are retained.

There is virtually no new physics in the further evaluation of the 3SM model. One has to evaluate a superoperator of the problem, the latter having the matrix elements,[2,4–6]

$$\mathbf{R}(ss' m_e m_g m_e' m_g')=\delta(m_e m_e')\delta(m_g m_g')W_{ss'}(\overline{q})+i\delta(ss')H_s^x(m_e m_g m_e' m_g'), \quad (19)$$

and to calculate eigenvalues and left and right eigenvectors of the superoperator $\hat{\mathbf{R}}$. Here $W_{ss'}(\overline{q})$ stands for the matrix element of the total diffusivity/relaxation operator $\hat{W}$. Eigenvalues and eigenvectors follow the set of equations

$$\hat{v}\hat{\mathbf{R}}\hat{u}=\hat{\lambda}, \quad \hat{v}\hat{u}=\hat{1}, \quad \hat{\mathbf{R}}\overline{u_\nu}=\lambda_\nu\overline{u_\nu}, \quad \text{and} \quad \overline{v_\nu}\hat{\mathbf{R}}=\overline{v_\nu}\lambda_\nu, \quad (20)$$

where $\hat{1}$ stands for the unit operator, $\hat{v}$ for the matrix of the left eigenvectors (an eigenvector $\overline{v_\nu}$ belonging to a particular eigenvalue λ_ν constitutes a row of the above matrix), $\hat{u}$ stands the matrix of the right eigenvectors (an eigenvector $\overline{u_\nu}$ belonging to a particular eigenvalue λ_ν constitutes a column of the above matrix), and $\hat{\lambda}$ for a diagonal matrix having subsequent eigenvalues as the diagonal elements. Subsequent complex eigenvalues $\lambda_\nu=\lambda_\nu(\overline{q})$ are labeled by the index

$$\nu = 1,2,\ldots,3(2I_e+1)(2I_g+1).$$

Hence a Mössbauer spectrum could be calculated in the same way as outlined in Ref. 2, except for the unnormalized line intensities [see Eq. (32) of Ref. 2], which have to be weighted by the unequal occupancies of various sites. Thus the above-mentioned intensities (complex numbers for the 3SM model) take on the following form presently:[2,10]

$$C_\nu(\overline{q}) = \sum_{k=\pm 1} \sum_{m_e m_e'} \sum_{m_g m_g'} \sum_{LL'} \delta_L \delta_{L'} \langle L' m_g' | \hat{T}_{pk}(\theta\phi) | m_e' \rangle^\star \times \langle L m_g | \hat{T}_{pk}(\theta\phi) | m_e \rangle \times \sum_{ss'} p_s f_{ss'}(\overline{q}) v_{\nu s' m_e' m_g'}(\overline{q}) u_{s m_e m_g \nu}(\overline{q}), \quad (21)$$

where all the symbols have the same meaning as in Ref. 2 except for the p_s defined by expressions (9) and (13); $f_{ss'}(\overline{q})$ defined by expression (18); and left eigenvector elements $v_{\nu s' m_e' m_g'}(\overline{q})$ and right eigenvectors elements $u_{s m_e m_g \nu}(\overline{q})$, the latter two defined by the set of equations (20). It has to be stressed that imaginary parts of the eigenvalues $\mathrm{Im}[\lambda_\nu(\overline{q})]$ represent spectral line positions, while real parts are responsible for the broadening, the latter taking on the value $2|\mathrm{Re}[\lambda_\nu(\overline{q})]|$ in comparison to the unbroadened linewidth.

In order to illustrate a behavior of the 3SM model, an example has been evaluated. Nuclear spins were chosen as $I_e = \frac{3}{2}$ and $I_g = \frac{1}{2}$. All frequencies and hyperfine levels were rescaled by q_0^{-1}, with $q_0 = 7.30254$ Å^{-1} (14.4 keV). ω_c and ω_v were set to zero. $p_\infty^{(3)} = p_0^{(3)}$ was chosen. Bragg conditions were chosen for the (R) sublattice, i.e., the $\overline{q} = G$ condition was chosen with G being one of the reciprocal lattice vectors of the (R) sublattice. Finally the following hyperfine parameters have been set: $A_{xx} = -0.1281$ mm/s [a quadrupole coupling constant along the x axis on the (RW) site]; $A_{zz} = -0.2379$ mm/s [a quadrupole coupling constant along the z axis on the (RW) site]; $S = -0.3$ mm/s [shift on the (R) site]; $A_{xx}^{(3)} = 0.2489$ mm/s [a quadrupole coupling constant on the (C) site]; and $S^{(3)} = -0.25$ mm/s [shift on the (C) site]. The above values of the hyperfine parameters are typical of the Fe^{3+} impurities in the insulators. Due to the fact that occupancy of the (C) site has been chosen as time independent, a frequency ω_1 could be determined from relationship (10) in terms of ω_D and $p_\infty^{(3)}$. Eigenvalues of the above model have been calculated versus ω_D for $p_\infty^{(3)} = 10^{-5}$ (almost a 2SM model), $p_\infty^{(3)} = \frac{1}{2}$, and $p_\infty^{(3)} \Rightarrow 1$ [almost pure diffusivity along channels with practically no impurities on the (R) sites]. Due to the fact that both nuclear spins are odd, all eigenvalues are fourfold degenerate (Kramers degeneracy), and one can expect six distinctly different eigenvalues at most. For the Bragg conditions chosen all broadenings are caused solely by the relaxation processes.

Figure 2 shows broadenings and corresponding positions for the model outlined above. One can see, that for a limiting case of the 2SM model [Fig. 2(a)], broadenings are doubly degenerated (in fact, they are eightfold degenerate), with all the intensity concentrated at broadenings marked with the dots (two almost indistinguishable widths at low frequency and a single broadening at a high frequency, the latter motionally narrowed). Extremely broad lines do not carry any intensity and, hence, they can be treated as ''ghost'' solutions. All broadenings tend to zero, of course, in the static limit. There are four line positions for this case (two doublets in the static limit), however, all the intensity is concentrated in the lines marked at both ends with dots. The latter lines evolve in such a way to produce in the high-frequency limit a doublet corresponding to the average EFG of (RW) and (RB) sites. An inset shows which broadenings contribute to the particular position at each zone. A semicolon indicates nonuniqueness of the solution (due to the degeneracy); i.e., those elements of the table which contain a semicolon could be interchanged one with another within a particular zone without affecting the physics. Underlined numbers indicate broadenings with the surviving intensity in the high-frequency limit.

Figure 2(b) is much more complex as it shows all the features of the 3SM model. It can be seen again that in the high-frequency limit all the intensity is carried by the motionally narrowed broadenings (marking dots), and concentrated in the ''inner doublet'' (dots). Six distinct line positions are produced for some region of the ω_D frequency and up to five distinct broadenings appear.

Figure 2(c) is extremely simple. Lines remain unbroadened (dots), positions do not depend upon ω_D and all the intensity is carried by the ''inner doublet'' belonging here to the (C) sites (dots). Such a behavior is quite clear, as all the impurities stay within the (C) sublattice, and there is no relaxation as all (C) sites are equivalent. All these models have the same eigenvalues in the static limit, of course.

Due to the fact that the relaxation operator $\hat{W}_R$ is non-Hermitian and it remains fully correlated to the non-Hermitian diffusivity operator $\hat{W}_D$,[8,9] the latter being dependent upon the wave-vector transfer, spectral line positions become dependent upon the wave-vector transfer; i.e., a spectrum shape depends on the emitted γ-ray direction in a more complex way than a simple broadening of the components.

III. THERMODYNAMICS OF THE 3SM MODEL

In order to obtain realistic results, one has to consider thermodynamical properties of the parent and daughter impurities. Mössbauer atoms are quite heavy and hence, all the diffusive motions are over the barrier jumps of the classical particles. Figure 3 shows energy levels and energy barriers relevant to the 3SM model. All the barriers are shown for the daughter impurity and they have to be positive in the stable system. An energy level U_C describes the energy difference for the daughter atom in the (C) site as compared to the energy of the daughter atom in the (R) site. A level U_C^0 does the same for the parent atom. These two levels do not need to be the same for different parent and daughter elements (they are practically the same for different isomeric states of the nucleus), and they can be either positive or negative depending upon the combination of the host and impurity elements; i.e., U_C and U_C^0 can be either positive or negative, and what is more U_C can be greater than, equal to, or less than U_C^0.

Hence the following set of equations holds, provided parent impurities are equilibrated with the system (for long living parents and temperatures that are not too low, the last assumption is obeyed quite well):

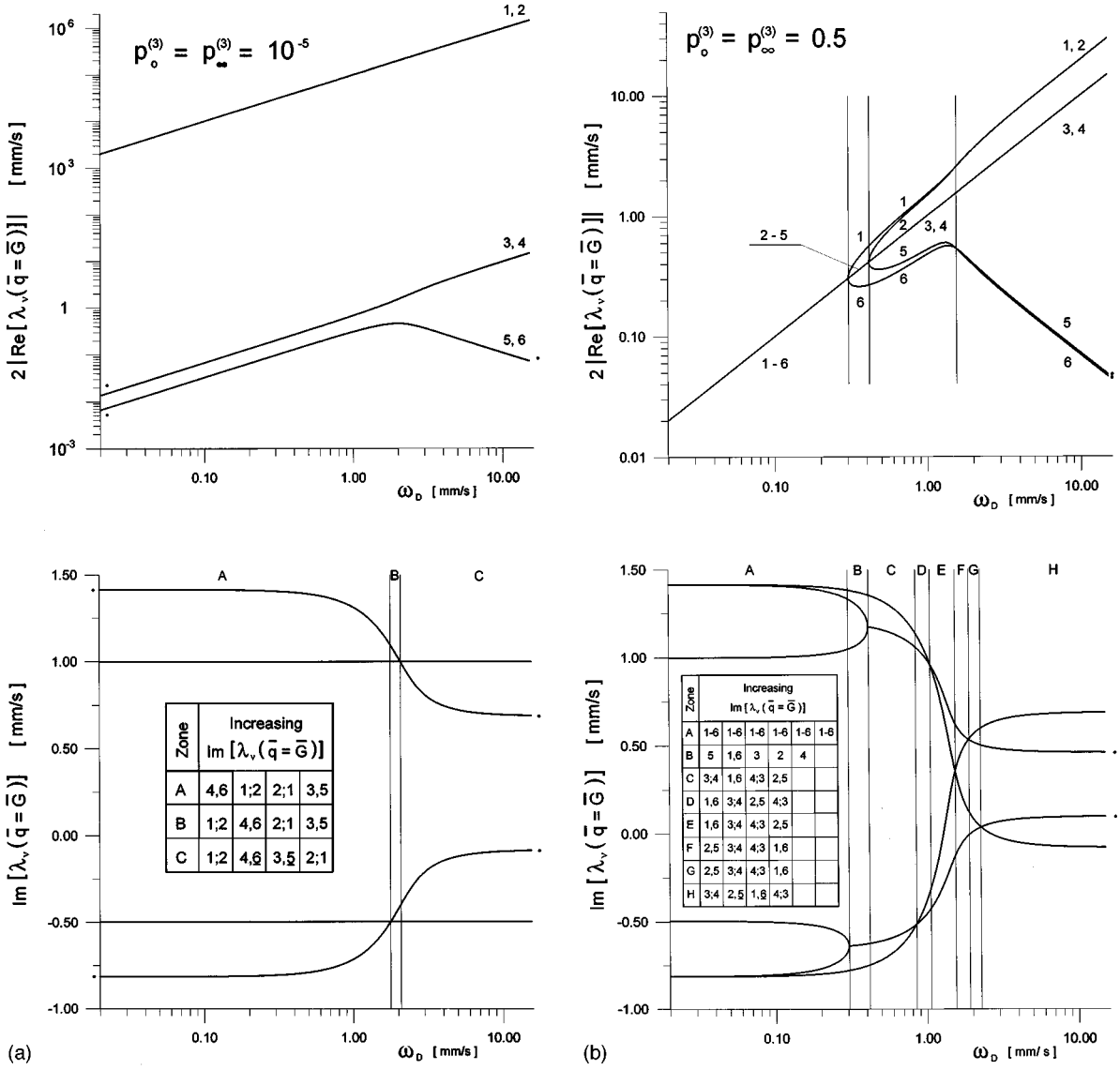

Zone	Increasing $\mathrm{Im}[\lambda_v(\bar{q}=\bar{G})]$			
A	4,6	1;2	2;1	3,5
B	1;2	4,6	2;1	3,5
C	1;2	4,6	3,5	2;1

Zone	Increasing $\mathrm{Im}[\lambda_v(\bar{q}=\bar{G})]$				
A	1-6	1-6	1-6	1-6	1-6
B	5	1,6	3	2	4
C	3;4	1,6	4;3	2,5	
D	1,6	3;4	2,5	4;3	
E	1,6	3;4	4;3	2,5	
F	2,5	3;4	4;3	1,6	
G	2,5	3;4	4;3	1,6	
H	3;4	2,5	1,6	4;3	

FIG. 2. Broadenings (upper diagrams) and line positions within the 3SM model. Broadenings are numbered from the largest to the smallest. Dots indicate broadenings or positions with the nonvanishing intensities. If no dot is shown, it means that all broadenings or positions contribute to the spectrum. Insets show which broadenings contribute to a particular position. Rows represent zones labeled *A*, *B*, etc., while columns represent positions in increasing order. Underlined numbers indicate which broadenings survive for $\omega_D \Rightarrow \infty$, while a semicolon indicates the nonuniqueness of the solution; i.e., within a given zone table elements containing a semicolon could be interchanged. For more details, see the text. (a) Broadenings and positions plotted vs ω_D for a 2SM limit. (b) Broadenings and positions plotted vs ω_D for equal populations of the (R) and (C) sublattices. (c) Broadenings and positions plotted vs ω_D for impurities occupying solely the (C) sublattice. Positions are labeled by the broadenings contributing to a particular position.

$$p_\infty^{(3)} = (2\exp[-U_C/(k_BT)])/(1+2\exp[-U_C/(k_BT)]), \tag{22}$$

$$p_0^{(3)} = (2\exp[-U_C^0/(k_BT)])/(1+2\exp[-U_C^0/(k_BT)]),$$

$$\omega_D = 8\omega^0 \exp[-U/(k_BT)] \quad \text{with}$$

$$\omega^0 = \tfrac{1}{8}\omega_D^0 \text{ of the 2SM (Ref. 2)},$$

$$\omega_1 = 4\omega^0 \exp[-(U-U_C)/(k_BT)],$$

$$\omega_c = \omega_c^0 \exp[-U_c/(k_BT)],$$

$$\omega_v = \omega_c^0 \exp[-U_v/(k_BT)],$$

$$\omega_0 = \omega_v^0 \exp[-U_0/(k_BT)],$$

$$R = \tfrac{1}{2}(\omega_v^0/\omega^0)\exp[-(U_0-U+U_C)/(k_BT)],$$

where k_B stands for the Boltzmann constant and T for the ambient temperature. Here U is a barrier for a jump from (R) to (C), U_0 is a barrier for a jump along the channel, U_c is a barrier for a jump from a channel to another channel in the tetragonal plane, and U_v is a barrier for a jump from a channel to another channel with a ''vertical'' component. A preexponential factor ω^0 [or equivalently ω_D^0 of the 2SM model (Ref. 2)] has to be the same for ω_D and ω_1 frequencies, as these frequencies are related one to another by expression (10). Preexponential factors for ω_c and ω_v jumps

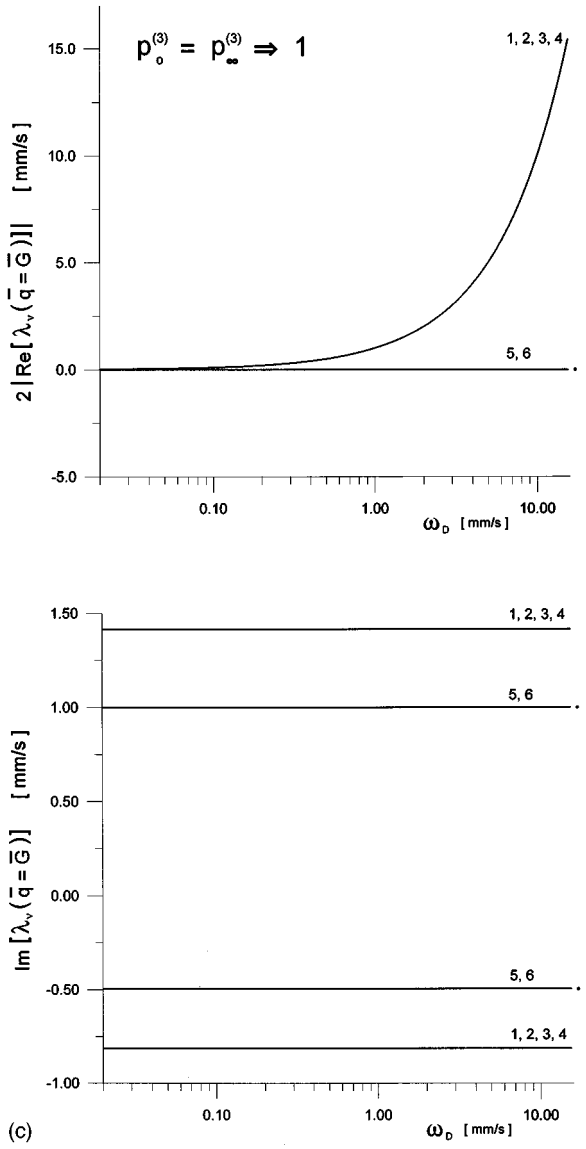

FIG. 2. (*Continued*).

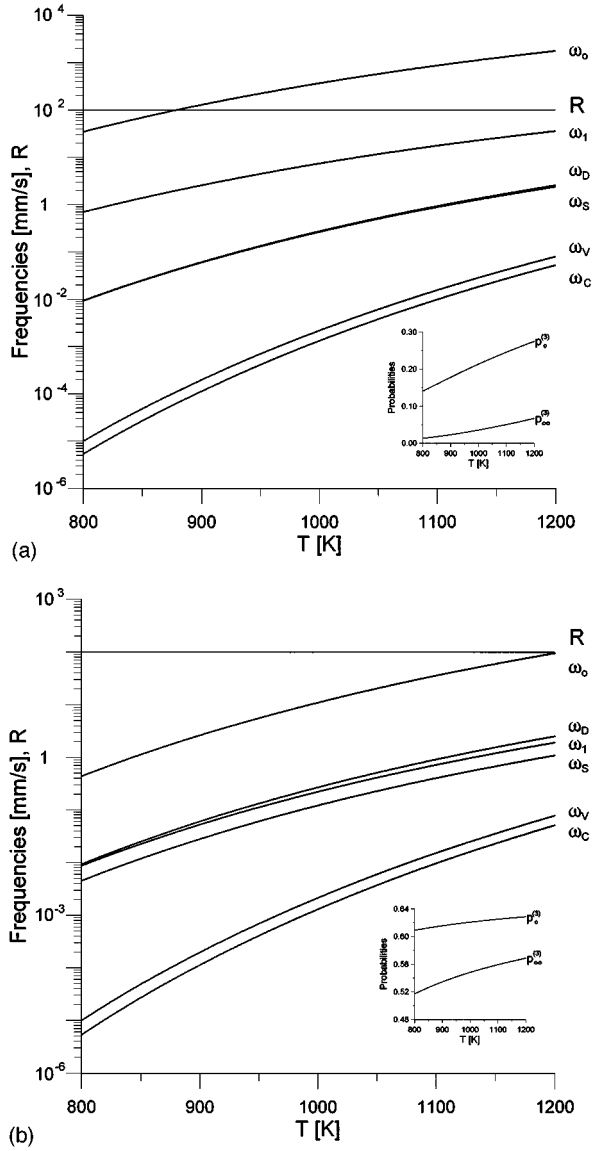

FIG. 4. Frequencies, R, and probabilities plotted vs temperature. See text for details. (a) Case I. (b) Case II.

are equal to each other (factor ω_c^0), as both these jumps originate from the same site in the same direction [see Fig. 1(c)]. A preexponential factor ω_v^0 describing ω_0 jumps along the channel is likely to be similar to the ω_c^0 factor, as both of them describe jumps over the empty lattice. On the other hand, a factor ω^0 has to be much smaller, as it describes correlated jumps due to the predominantly interstitialcy mechanism. Sasaki, Peterson, and Hoshino[1] found, by the tracer method, that the R factor is close to 100 and almost temperature independent for Fe diluted in TiO_2 rutile. Hence one can conclude that for the latter case $U \cong U_0 + U_C$ and $(\omega_v^0/\omega^0) \cong 200$.

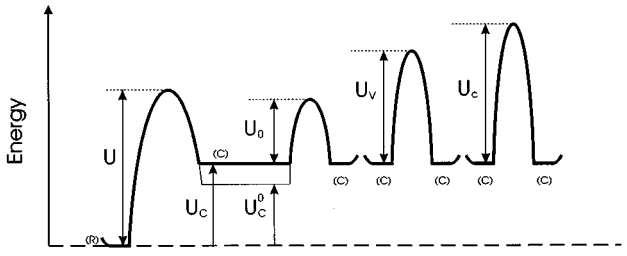

FIG. 3. Energy levels and jump barriers of the 3SM model. See text for details.

On the other hand, it is very likely that barriers U_c and U_v are much higher than the remaining barriers due to the geometrical conditions. A barrier U_c has to be higher than U_v, as the jump associated with the U_c barrier has a route much closer to the host cation-anion bond.[2,11] Usually an oxygen parameter u (Fig. 1), i.e., a ratio of the host cation-anion bond length to the $a\sqrt{2}$ distance, takes on a value of about 0.3. Hence the ω_c route goes over the bond at a $\frac{1}{4}c$ distance from the bond axis. Figure 4 shows two examples evaluated in accordance with the above set of equations. All frequencies have been rescaled by q_0^{-1}, with $q_0 = 7.30254$ Å^{-1} (14.4 keV), and the following values have been adopted for various parameters:

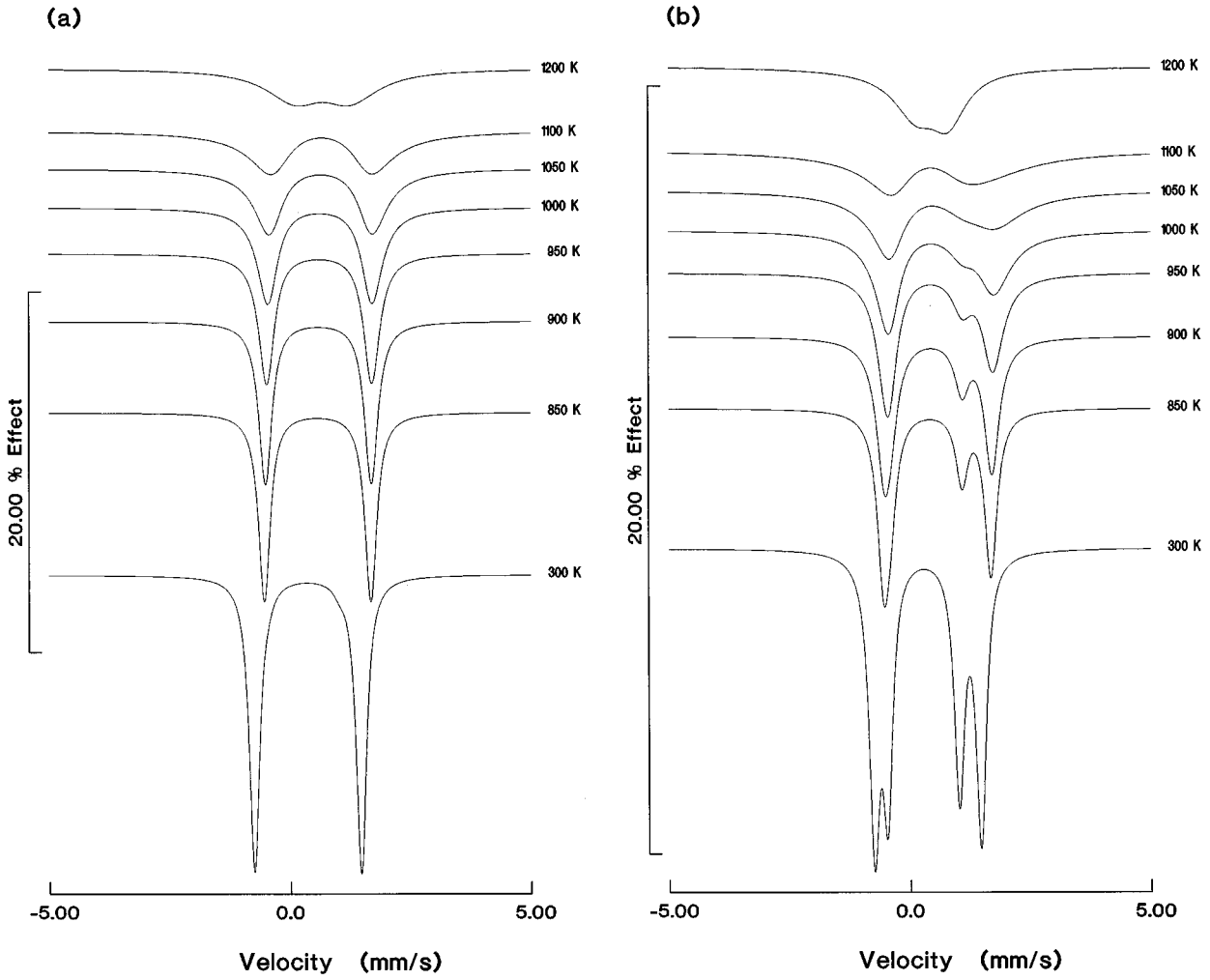

FIG. 5. Mössbauer spectra plotted vs linear velocity scale for various temperatures. See text for details. (a) Case I. (b) Case II.

$$\omega^0 = 2.339\times 10^4 \text{ mm/s}, \quad \omega_c^0 = \omega_v^0 = 4.660\times 10^6 \text{ mm/s},$$

$U = 13\,456$ K, $U_c = 22\,000$ K, $U_v = 21\,500$ K,
$U_C = 4000$ K, $U_C^0 = 2000$ K, $U_0 = 9450$ K (case I),
$U_C = 500$ K, $U_C^0 = 200$ K, $U_0 = 12\,950$ K (case II).

The above values have been adopted in such a way to obtain an almost temperature-independent $R \cong 100$, and to reproduce results of the 2SM model at 1200 K for $R = 100$ (see Ref. 2). Figure 4(a) shows resulting frequencies R and probabilities for case I, while Fig. 4(b) shows the same results for case II. It has to be noted that case I is much closer to the 2SM model than case II [see e.g., closeness of ω_D and ω_S in Fig. 4(a)].

Hence one can conclude this Section by saying that the 3SM model is able to explain the constancy of the R ratio versus temperature, and that for such cases the actual value of the ratio R could be used to evaluate properties of the correlated dynamics of the interstitialcy jumps.

IV. EXAMPLES OF SPECTRA

In order to illustrate the influence of the diffusive jumps and correlated relaxation of the EFG and shifts, some emission Mössbauer spectra have been calculated for a 14.4-keV line of ^{57}Fe having a parent isotope ^{57}Co and embedded in a single crystal of TiO_2 rutile. A detailed procedure was already described in Ref. 2. All ''instrumental'' parameters and parameters describing the ''internal'' behavior of the (RW) and (RB) sites have been taken from Ref. 2. All frequencies and probabilities have been taken either for the above-outlined case I or for case II. The following parameters have been adopted for the (C) site (frequency parameters rescaled by q_0^{-1} with $q_0 = 7.30254$ Å^{-1}):

$A_{xx}^{(3)} = 0.2489$ mm/s and taken as temperature independent,

$$S^{(3)} = -0.25 \text{ mm/s} \quad \text{at } T = 0 \text{ K},$$

$$B_{xx}^{(3)} = 1.300\times 10^{-2} \text{ Å}^2 \quad \text{at } T = 0 \text{ K},$$

$$B_{zz}^{(3)} = 1.927\times 10^{-3} \text{ Å}^2 \quad \text{at } T = 0 \text{ K},$$

$\Gamma_0 = 0.097$ mm/s as a natural linewidth (constant).

A quadrupole coupling constant $A_{xx}^{(3)}$ for the excited nuclear state (the ground state is a Kramers doublet) has been estimated by a charge cluster method applying the best available value for the oxygen parameter $u = 0.3049$,[11,12] the latter further corrected for the charge in the Ti-O bond.[13] A quad-

rupole coupling constant is likely to be very weakly temperature dependent as the oxidation state is unlikely to change upon transfer from the (R) to the (C) site. On the other hand, quadrupole interactions are almost temperature independent on the (R) sites.[2] Hence, an isomer shift should be almost the same on the (R) and (C) sites and the difference is mainly due to the second-order Doppler shift.[2] Thus a rough estimate gives the above-mentioned value for $S^{(3)}$ at $T=0$ K. A shift has been corrected solely for the second order Doppler shift versus increasing temperature by using a Debye density of the phonon states with the Debye temperature $\theta_D=600$ K (Refs. 2, 11, and 14) and a mean-squared velocity:

$$\langle v^2\rangle_3 = 1.793\times 10^{10}\ \ (\mathrm{mm/s})^2 \quad \text{at}\ \ T=0\ \ \mathrm{K}.$$

The above value has been roughly estimated comparing volumes accessible to the impurity in the (R) and (C) sites, respectively. The value for the (R) site has been already estimated previously.[2]

The same density of the phonon states has been used to correct mean-squared displacements $B_{xx}^{(3)}$ and $B_{zz}^{(3)}$. There is no simple way to estimate the above displacements at $T=0$ K. Hence a displacement in the tetragonal plane, i.e., $B_{zz}^{(3)}$, has been taken as the average of the displacements in the tetragonal plane for the (R) site,[2] while the value along the tetragonal axis has been roughly estimated taking into account a local freedom of motion along the channel (in the vicinity of the potential minimum). Hence the latter value is much larger, leading to a significant anisotropy of the recoilless fraction at elevated temperatures at the (C) sites.

Spectra have been calculated for the direction of the emission of the γ ray, chosen in such a way to obtain almost minimal diffusional broadening, i.e., for the polar angle $\theta=35.6°$ and for the azimuthal angle $\phi=0°$.

Figure 5(a) shows spectra calculated for case I, while Fig. 5(b) spectra calculated for case II. Spectra at $T=300$ K have been calculated, taking $p_0^{(3)}$ from $T=500$ K, as below 500 K diffusivity is so slow that no equilibrium could be reached in a reasonable time period. The above spectra have been calculated for a perfect experimental geometry, i.e., for an acceptance angle of the detector tending to zero.

One can clearly see, in the static limit ($T=300$ K), two doublets [see Fig. 5(b)], the inner one originating from the site (C), and the outer one from site (R). The inner doublet is barely visible in Fig. 5(a), as case I is close to the 2SM model, the latter exhibiting no measurable signal from the (C) sites. Lines cannot be assigned to particular sites at elevated temperatures, as the superoperator mixes all sites.

A ''strange'' shape between 950 K and 1100 K for case II is caused partly by the dependence of the line positions on the wave-vector transfer as the Bragg conditions are not satisfied exactly for the direction chosen. One has to note, that for a given lattice and a fixed γ-ray energy, Bragg conditions usually cannot be satisfied exactly at all.[15] The chance for the Bragg conditions to be satisfied exactly diminishes with the increasing number of the Bravais sublattices involved in the diffusivity.[6] Due to the fact that an almost minimal diffusional broadening direction has been chosen, one can see a motional narrowing at the highest temperatures shown. All

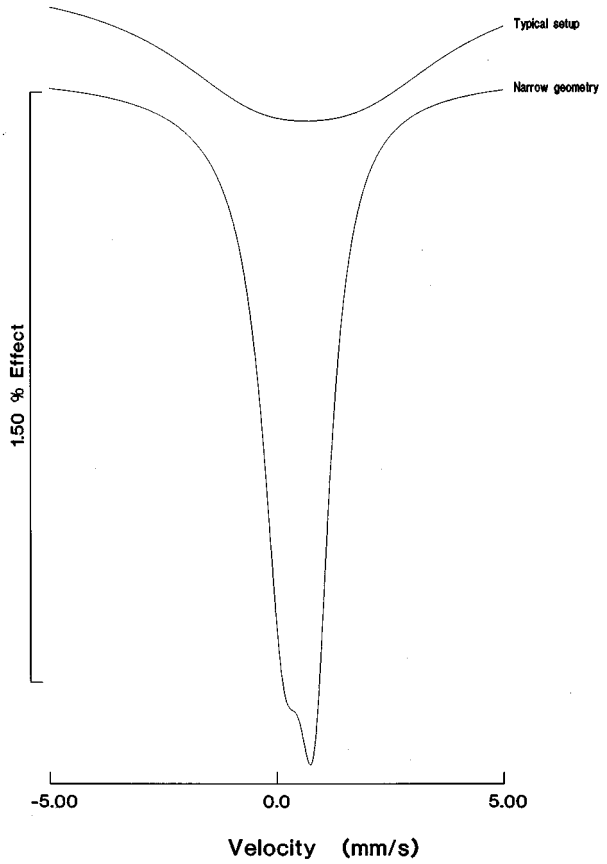

FIG. 6. A comparison of the case II spectrum at 1200 K for a perfect (narrow) geometry and for a typical setup. See text for details.

the above mentioned effects are more distinct for case II, as for the latter case more eigenvalues exhibit significant intensities.

Finally, Fig. 6 shows effects of the imperfect geometry for a case II spectrum at 1200 K, i.e., at a temperature high enough to have a very large broadening slightly off the direction exhibiting narrow spectra. The effect would be much lesser in other directions and at lower temperatures. Calculations have been performed for almost the same conditions as those of Ref. 2.

Roughly speaking, a typical setup consists of a rectangular source having dimensions 7×12 mm^2 and a thickness 0.1 mm. A direction $\langle 111\rangle$ is perpendicular to the source surface, and the source is located 120 mm beneath a circular collimator having 15-mm diameter. The source is rotated around the axis parallel to the collimator plane in such a way that a photon propagating along the collimator axis is emitted at the angles $\theta=35.6°$ and $\phi=0°$. The longer source dimension is parallel to the source rotation axis, while the rotation axis is located about 4 mm ''beneath'' the source, and has a common point with the collimator axis. It is assumed as well that impurities are evenly distributed within the source volume. Hence, for such sensitive directions, at elevated temperatures two-dimensional Soller collimators might be essential[17] to obtain reliable results or even to observe any signal at a reasonable statistics. A broadening due to imperfect geometry is particularly dramatic for the case shown, because line positions depend upon the wave-vector transfer (direction),

and the imperfect geometry causes some averaging over different wave-vector transfers (directions) within the acceptance angle of the detector. On the other hand, many eigenvalues have non-negligible intensities as the signal comes from (R) and (C) sites.

V. CONCLUSIONS

It has been shown that a previously developed 2SM model[2] could be extended into a 3SM model, the latter accounting for a signal coming from impurities in the channels. A 3SM model merges smoothly with the 2SM model in the case when a fraction of impurities in the channel becomes negligible, and direct jumps between various channels can be neglected; i.e., channels remain ''localized'' in the direction perpendicular to the tetragonal axis. Hence, a ''direct jump'' 3SM model has as a limiting case an event (encounter) 2SM model. This is the first known example, to our best knowledge, where such a ''transition'' has been shown to exist. Its presence, in our opinion, is a strong argument justifying the appropriateness of the encounter approximation under suitable conditions to evaluate data.

A superoperator of the 3SM model contains off-diagonal elements depending upon the wave-vector transfer, as some jumps occur between various Bravais sublattices. The same jumps are responsible for the relaxation of the EFG and the total spectral shift between sublattices involved. Hence, line positions become dependent upon the wave-vector transfer, i.e., upon a direction in the case of the Mössbauer spectroscopy. Superoperators having the above-mentioned properties have never been previously developed to our best knowledge. They are able to explain quite complex spectral patterns.

A 3SM model is basically a nonequilibrium model able to trace a redistribution of impurities upon decay from a parent to a daughter element provided a time window of the experimental method is comparable to the time interval needed to complete the above redistribution. A redistribution takes place when the parent energy on the (C) site as compared to the energy on the (R) site is significantly different from the same energy difference for the daughter element. For the 14.4-keV transition in ^{57}Fe (being a daughter of the ^{57}Co) a time window defined by $1/\Gamma_0$ equals 141.2 ns,[18] where Γ_0 denotes a natural linewidth of the Mössbauer level involved. Hence one sees a parent distribution in the case of the slow diffusivity limit, and a daughter distribution in the very fast diffusivity limit, provided an emission Mössbauer spectroscopy method is used. A model reproduces all intermediate situations as well. The highest sensitivity to redistribution occurs approximately for $\omega_S \cong \Gamma_0$. The sensitivity to redistribution is lost, of course, in the case of absorption spectroscopy, as for the latter case parent and daughter nuclei are simply different isomeric states of the same nucleus and the above-mentioned difference of the energy levels is negligible for various isomeric states.

Finally, it has to be stressed that for some directions on the Ewald sphere (at highly elevated temperatures), where the diffusional broadening is minimal and the motional narrowing of the relaxation processes takes place, a very careful design of the experimental geometry is required to obtain reliable data or even to observe any effect at all. This dramatic sensitivity of the spectral shape to the direction of observation is partly caused by the fact that line positions are wave-vector transfer (direction) sensitive. The effect is particularly strong for a significant fraction of impurities staying within a channel. It seems that the simplest remedy is the application of the two-dimensional Soller collimators for such cases.[17]

ACKNOWLEDGMENTS

We thank Dr. Wojciech Karaś, Department of Solid State Physics, University of Mining and Metallurgy, Cracow, Poland for an illuminating remark. This work was financed by KBN (The National Committee for Scientific Research, Poland) under Grant No. 2 P302 193 05.

*To whom all correspondence should be addressed. Electronic address: sfrueben@cyf-kr.edu.pl

[1] Jun Sasaki, N. L. Peterson, and K. Hoshino, J. Phys. Chem. Solids **46**, 1267 (1985).

[2] K. Ruebenbauer, U. D. Wdowik, and M. Kwater, Phys. Rev. B **54**, 4006 (1996).

[3] It has to be realized that in the absence of magnetic interactions all hyperfine interactions depend upon the even static electric multipole tensors, as the parity is conserved and the nucleus has a nonzero charge. Various (C) sites differ solely by the orientation of the odd tensors, and hence one is left solely with odd contributions to the recoilless fraction. The latter contributions do not affect eigenvalues of the problem, as they contribute to the intensities only. What is more, the above tensors appear under the exponential function and, hence, a thermodynamic average over all (C) sites contains solely even terms as all odd terms cancel each other exactly. Hence a Mössbauer nucleus is unable to distinguish between various (C) sites on the local scale, and the medium containing Mössbauer atoms is unable to polarize the emitted/transmitted γ-ray beam.

[4] M. Blume, Phys. Rev. **174**, 351 (1968).

[5] H. Winkler and E. Gerdau, Z. Phys. **267**, 61 (1974).

[6] M. Kwater, K. Ruebenbauer, and U. D. Wdowik, Physica B **190**, 199 (1993).

[7] J. W. Rowe, K. Sköld, H. E. Flotow, and J. J. Rush, J. Phys. Chem. Solids **32**, 41 (1971).

[8] R. Kutner and I. Sosnowska, J. Phys. Chem. Solids **38**, 741 (1977).

[9] R. Kutner and I. Sosnowska, Acta Phys. Pol. A **51**, 171 (1977).

[10] M. Kwater, K. Ruebenbauer, and U. D. Wdowik, Physica B **190**, 209 (1993).

[11] C. J. Howard, T. M. Sabine, and F. Dickson, Acta Crystallogr. B **47**, 462 (1991).

[12] W. Gonschorek, Z. Kristallogr. **160**, 187 (1982).

[13] E. F. Bertaut, J. Phys. (Paris) **39**, 1331 (1978).

[14] W. Potzel, in *Proceedings XX Zakopane Winter School on Physics*, edited by J. J. Bara, K. Ruebenbauer, and Z. Stachura (INP, Cracow, 1985), Vol. 2, p. 294.

[15] One has to realize that the ratio of the total spectral width to the γ-ray energy is usually less than 10^{-10}, a real part of the refraction index for nonresonant propagation is close to the unit operator for typical γ-ray energies involved (Ref. 6), and a reso-

nant self-absorption within the source can be neglected for highly diluted impurities (Ref. 16). Hence the absolute value of the wave-vector transfer, the latter being an absolute value of the wave vector of the quasielastically emitted γ ray, is practically a very well-defined constant.

[16] R. A. Wagoner, B. Bullard, M. May, S. Dickson, and J. G. Mullen, Hyperfine Interact. **58**, 2687 (1990).

[17] J. G. Mullen (private communication).

[18] In principle, Γ_0 might be site dependent due to the slightly different electron charge densities at a nucleus for various sites and, hence, various internal conversion coefficients. However, the variability is extremely small (and it could be neglected) due to the fact that inner shells are practically unaffected, and, on the other hand, the inner shells are mainly responsible for the overall internal conversion coefficient.